

## EFFECTS OF BARYON DISSIPATION ON THE DARK MATTER VIRIAL SCALING RELATION

ERWIN T. LAU<sup>1</sup>, DAISUKE NAGAI<sup>2,3</sup>, ANDREY V. KRAVTSOV<sup>1,4</sup>  
The Astrophysical Journal, submitted

### ABSTRACT

We investigate effects of baryon dissipation on the dark matter virial scaling relation between total mass and velocity dispersion and the velocity bias of galaxies in groups and clusters using self-consistent cosmological simulations. We show that the baryon dissipation increases the velocity dispersion of dark matter within the virial radius by  $\approx 5 - 10\%$ . The effect is mainly driven by the change in density and gravitational potential in inner regions of cluster, and it is larger in lower mass systems where gas cooling and star formation are more efficient. We also show that the galaxy velocity bias depends on how galaxies are selected. Galaxies selected based on their stellar mass exhibit no velocity bias, while galaxies selected based on their total mass show positive bias of  $\approx 10\%$ , consistent with previous results based on collisionless dark matter-only simulations. We further find that observational estimates of galaxy velocity dispersion are unbiased with respect to the velocity dispersion of dark matter, provided galaxies are selected using their stellar masses and their velocity dispersions are computed with more than twenty most massive galaxies. Velocity dispersions estimated with fewer galaxies, on the other hand, can lead to significant underestimate of dynamical masses. Results presented in this paper should be useful in interpreting high-redshift groups and clusters as well as cosmological constraints derived from upcoming optical cluster surveys.

*Subject headings:* cosmology: theory—clusters: formation— methods: numerical

### 1. INTRODUCTION

Galaxy clusters are unique laboratories for astrophysics and powerful probes in cosmology. As the largest and most massive gravitationally-bound structures in the universe, they provide well-defined environments for studies of various astrophysical processes: e.g., plasma interactions in the intracluster medium, galaxy interactions and evolution, supermassive black hole feedback processes, etc. In the cosmological context, galaxy clusters are good tracers of the cosmological evolution, as their overall dynamics are largely driven by gravity (Kaiser 1986, see Voit 2005 for a review). Different ways in which clusters can be used for cosmology rely on understanding of how their observable properties are related to the total virialized mass. One of the main challenges of cluster cosmology and astrophysics are thus understanding this relation and accurate measurements of cluster mass in observations.

Dynamical mass estimate uses motions of cluster galaxies as tracers of the mass distribution of groups and clusters, and it is a relatively inexpensive and efficient technique. The first dynamical measurement of cluster mass dates back to the pioneering works of Zwicky (1933, 1937) and Smith (1936, see Biviano 2000 for a historical overview). To date, a variety of dynamical mass estimation techniques has been devised and used extensively, including the projected mass estimator (Heisler et al. 1985; Rines et al. 2003; Rines & Diaferio 2006), the Jeans analysis (Carlberg et al. 1997; Girardi et al. 1998; van der Marel et al. 2000; Biviano & Girardi 2003; Rines et al. 2003; Katgert et al. 2004; Biviano & Poggianti 2009), and the caustic method (Diaferio & Geller 1997; Diaferio 1999; Biviano & Girardi 2003; Rines et al. 2003;

Rines & Diaferio 2006; Rines et al. 2007; Diaferio et al. 2005). For low-mass clusters and groups ( $M \lesssim 10^{14} M_{\odot}$ ), especially at higher redshifts, dynamical mass estimate is often the only available approach to obtain mass (e.g., Coil et al. 2006), since they are mostly X-ray dim and not massive enough to be detected by the Sunyaev-Zeldovich effect. Dynamical mass estimates also provide important check on mass measurements obtained using other methods and help in calibration of optical mass-richness relation (e.g. Becker et al. 2007).

Recently, Evrard et al. (2008) used a large set of dissipationless  $N$ -body cosmological simulations (some with non-radiative gasdynamics) and showed that virial scaling relation for dark matter particles is consistent with predictions of the virial theorem, in which the velocity dispersion scales with halo mass to the power of  $1/3$ . Their study further showed that the virial scaling relation exhibits remarkable degree of universality and self-similarity across a broad range of halo masses, redshifts, and cosmological models, as well as having very small scatter. This is good news for the use of optical clusters as sensitive cosmological probes.

In practice, however, applying the virial scaling relation for precision cosmology faces a number of difficulties. First, unbiased selection of cluster member galaxies (i.e., removal of foreground and background interlopers) is difficult and can be a major source of systematic uncertainty in velocity dispersion measurement of cluster members (see e.g., McKay et al. 2002; Biviano et al. 2006; Chen et al. 2006), especially for low-mass clusters and groups consisting of only a few bright galaxies (e.g., Hernquist et al. 1995). Second, since we can only measure the line-of-sight velocity, velocity anisotropy of galaxies is also an additional source of systematic uncertainty (e.g., Biviano & Poggianti 2009). In order to use velocity dispersion as an accurate and precise tracer of cluster mass for future optical cluster surveys, it is imperative to understand and control these uncertainties.

However, even if cluster member selection and velocity anisotropies are well understood and controlled, we need

<sup>1</sup> Department of Astronomy and Astrophysics, 5640 South Ellis Ave., The University of Chicago, Chicago, IL 60637 (ethlau@oddjob.uchicago.edu)

<sup>2</sup> Department of Physics, Yale University, New Haven, CT 06520

<sup>3</sup> Yale Center for Astronomy & Astrophysics, Yale University, New Haven, CT 06520

<sup>4</sup> Kavli Institute for Cosmological Physics and Enrico Fermi Institute, 5640 South Ellis Ave., The University of Chicago, Chicago, IL 60637

to understand possible systematic uncertainties in the intrinsic relation between three-dimensional velocity dispersion of galaxies and total cluster mass. For example, the simulations used in the study of Evrard et al. (2008) did not include effects of dissipative baryonic processes, which do accompany cluster formation and lead to formation of cluster galaxies. From a number of X-ray observations we know that self-similarity is broken in cluster cores and group-size systems and this causes deviations of scaling relations from theoretical predictions of cluster formation where gravity is the only energy driver (e.g., Markevitch 1998; Arnaud & Evrard 1999; Osmond & Ponman 2004; Pratt et al. 2009). Baryon dissipation, in particular, modifies the total mass profile and, likely, the velocity dispersion profile in groups and clusters both due to the contraction and deepening of cluster potential (e.g., Zeldovich et al. 1980; Blumenthal et al. 1986; Gnedin et al. 2004; Sellwood & McGaugh 2005) and due to the overall redistribution of baryonic mass (e.g., Rudd et al. 2008). Observationally, we can only measure velocity dispersions of cluster galaxies, which can be a biased tracer of dark matter velocity dispersion. This *velocity bias* is also a potential source of systematic uncertainties (e.g., Carlberg et al. 1990; Evrard et al. 1994; Frenk et al. 1996; Colín et al. 2000; Ghigna et al. 2000; Springel et al. 2001; Diemand et al. 2004; Gao et al. 2004; Faltenbacher et al. 2005; Biviano et al. 2006; Faltenbacher & Diemand 2006).

In this paper, we focus on the latter two intrinsic systematic uncertainties. Namely, we investigate the effect of dissipation on the dark matter virial scaling relation and velocity bias of cluster galaxies using high resolution self-consistent cosmological cluster simulations. We show that the baryon dissipation increases the velocity dispersion of dark matter, by changing the inner density profiles and potential of gravitationally bound systems, and that the effects are larger in lower mass systems where gas cooling and star formation are more efficient. We also show that observational estimate of dynamical mass gives unbiased mass estimate of galaxy groups and clusters, in contrary to the previous results obtained based on dark matter only simulations. We describe our simulations in § 2 and report results in § 3. Main results are summarised in § 4.

## 2. THE SIMULATION

In this study, we analyze high-resolution cosmological simulations of 16 cluster-sized systems performed using the Adaptive Refinement Tree (ART)  $N$ -body+gasdynamics code (Kravtsov 1999; Kravtsov et al. 2002). The ART is a Eulerian code that uses adaptive refinement in space and time, and (non-adaptive) refinement in mass (Klypin et al. 2001) to reach the high dynamic range required to resolve cores of halos formed in self-consistent cosmological simulations. The simulations presented here are discussed in detail in Nagai et al. (2007a) and Nagai et al. (2007b) and we refer the reader to these papers for more details. Here we highlight aspects of the simulations relevant for this work.

The  $N$ -body+gasdynamics cluster simulations used in this analysis include collisionless dynamics of dark matter and stars, and gasdynamics. In order to assess the effects of gas cooling and star formation on the dynamics of dark matter, we conducted each cluster simulation with two different prescriptions for gasdynamics: one with only the standard gasdynamics for the baryonic component without radiative cooling and star formation - the ‘non-radiative’ (NR) runs, and ‘cooling+SF’ (CSF) runs. In the CSF runs, several physical

TABLE 1  
PROPERTIES OF THE SIMULATED CSF CLUSTERS AT  $z = 0$

| Cluster ID  | $r_{200c}$<br>[ $h^{-1}$ Mpc] | $M_{200c}$<br>[ $10^{14} h^{-1} M_{\odot}$ ] | $N(< r_{200c})$ |
|-------------|-------------------------------|--|-----------------|
| CL101 ..... | 1.786                         | 13.2   | 1243854         |
| CL102 ..... | 1.509                         | 7.98   | 749369          |
| CL103 ..... | 1.585                         | 9.24   | 867435          |
| CL104 ..... | 1.435                         | 6.87   | 633240          |
| CL105 ..... | 1.443                         | 7.00   | 649012          |
| CL106 ..... | 1.316                         | 5.30   | 496021          |
| CL107 ..... | 1.174                         | 3.76   | 348465          |
| CL3 .....   | 1.104                         | 3.13   | 981098          |
| CL5 .....   | 0.925                         | 1.84   | 574968          |
| CL6 .....   | 0.958                         | 2.05   | 644496          |
| CL7 .....   | 0.937                         | 1.91   | 603447          |
| CL9 .....   | 0.657                         | 0.66   | 204249          |
| CL10 .....  | 0.710                         | 0.83   | 261205          |
| CL11 .....  | 0.779                         | 1.09   | 338860          |
| CL14 .....  | 0.755                         | 1.00   | 312626          |
| CL24 .....  | 0.671                         | 0.70   | 221012          |

processes critical to various aspects of galaxy formation are included: star formation, metal enrichment and thermal feedback due to supernovae Type II and Type Ia, self-consistent advection of metals, metallicity dependent radiative cooling and UV heating due to cosmological ionizing background (see Nagai et al. (2007a) for details of the metallicity-dependent radiative cooling and star formation). These simulations therefore follow the formation of galaxy clusters starting from the well-defined cosmological initial conditions and capture the dynamics and properties of the ICM in a realistic cosmological context. However, some potentially relevant physical processes, such as AGN bubbles, magnetic field, and cosmic rays, are not included. Therefore, the simulated cluster properties are probably not fully realistic in the innermost cluster regions, where these processes are likely important.

Our simulated sample includes 16 clusters at  $z = 0$  and their most massive progenitors at  $z = 0.6$  and  $z = 1.0$ . The properties of simulated clusters at  $z = 0$  are given in Table 1. The total cluster masses are reported at the radius  $r_{200c}$  enclosing overdensities with respect to the critical density at the redshift of the output (below, we also use a higher overdensity level, 500). The dark matter (DM) particle mass in the region around the cluster was  $9 \times 10^8 h^{-1} M_{\odot}$  for CL101-107 and  $3 \times 10^8 h^{-1} M_{\odot}$  for CL3-24, while other regions were simulated with lower mass resolution. The peak resolution of the cluster simulation is  $\approx 2 - 3 h^{-1}$  kpc in the box size of  $80-120 h^{-1}$  Mpc. The simulations are performed for the flat  $\Lambda$ CDM model:  $\Omega_m = 1 - \Omega_{\Lambda} = 0.3$ ,  $\Omega_b = 0.04286$ ,  $h = 0.7$  and  $\sigma_8 = 0.9$ , where the Hubble constant is defined as  $100h$  km s $^{-1}$  Mpc $^{-1}$ , and an  $\sigma_8$  is the power spectrum normalization on an  $8h^{-1}$  Mpc scale.

## 3. RESULTS

### 3.1. Virial Scaling Relation

Following Evrard et al. (2008), we assume velocity isotropy and calculate the one-dimensional dark matter velocity dispersion  $\sigma_{DM}$  to be

$$\sigma_{DM}^2 = \frac{1}{3N} \sum_{i=1}^3 \sum_{p=1}^N (v_{p,i} - \bar{v}_i)^2, \quad (1)$$

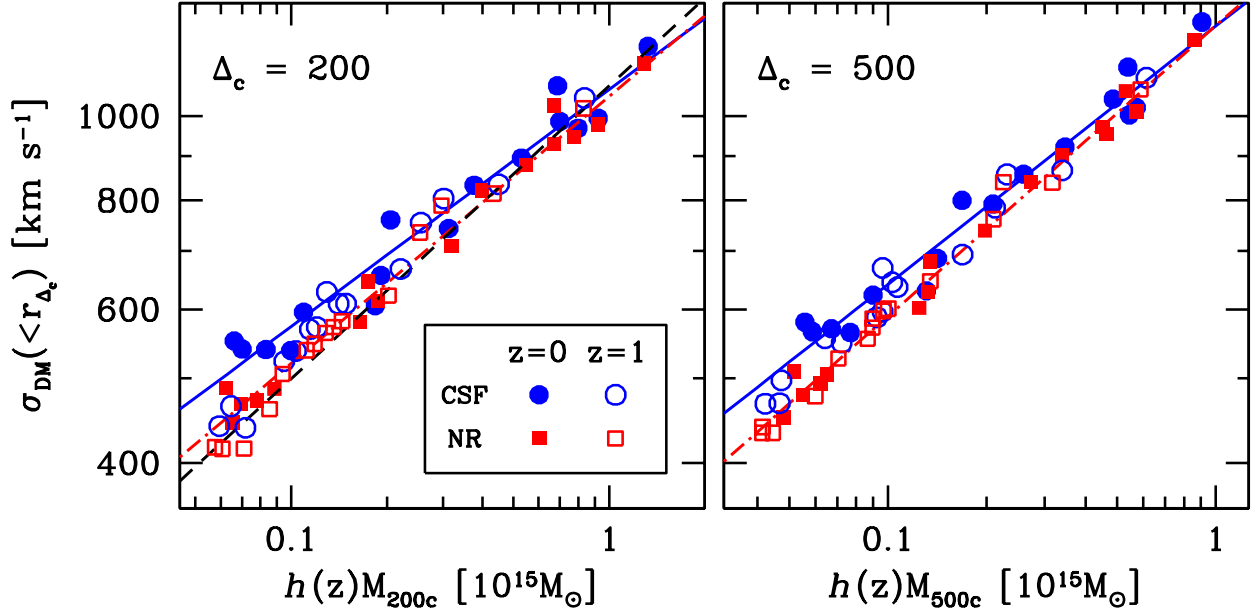


FIG. 1.— *Left* panel shows the dark matter virial scaling relation for the sixteen clusters for  $\Delta_c = 200$  using least-square fitting at  $z = 0$  and  $z = 1$  and the *right* panel shows the same relation for  $\Delta_c = 500$ . For each panel, the CSF clusters at  $z = 0$  are represented by the solid blue circles, and the CSF clusters at  $z = 1$  are represented by open blue circles. The solid blue line is the best least-square fit for the  $z = 0$ . For the NR run, the  $z = 0$  and  $z = 1$  clusters are represented by solid red squares and open red squares respectively, which the red dot-dashed line is the best least-square fit to the clusters at  $z = 0$ . For reference, the best fit from Evrard et al. (2008) is shown as black dashed line. Please refer to Table 2 for the values of the fitted parameters.

TABLE 2  
SCALING RELATION PARAMETERS

|   | $\Delta_c = 200$        |                         |                         |
|---|-------------------------|-------------------------|-------------------------|
|   | $z = 0.0$               | $z = 0.6$               | $z = 1.0$               |
| $\alpha$                                      | NR $0.3072 \pm 0.0114$  | CSF $0.3214 \pm 0.0246$ | CSF $0.3512 \pm 0.0152$ |
| $\sigma_{\text{DM},0}$ [km/s]                 | NR $643 \pm 7$          | CSF $648 \pm 11$        | CSF $645 \pm 8$         |
| $\langle \delta_{\ln \sigma}^2 \rangle^{1/2}$ | NR $0.0410 \pm 0.0079$  | CSF $0.0630 \pm 0.0086$ | CSF $0.0348 \pm 0.0062$ |
|   |                         |                         |                         |
|   | $\Delta_c = 500$        |                         |                         |
|   | $z = 0.0$               | $z = 0.6$               | $z = 1.0$               |
| $\alpha$                                      | NR $0.3335 \pm 0.0096$  | CSF $0.3256 \pm 0.0207$ | CSF $0.3475 \pm 0.0110$ |
| $\sigma_{\text{DM},0}$ [km/s]                 | NR $742 \pm 6$          | CSF $737 \pm 10$        | CSF $751 \pm 10$        |
| $\langle \delta_{\ln \sigma}^2 \rangle^{1/2}$ | NR $0.0310 \pm 0.0059$  | CSF $0.0444 \pm 0.0082$ | CSF $0.0258 \pm 0.0062$ |
|   | CSF $0.0459 \pm 0.0075$ | CSF $0.0394 \pm 0.0073$ | CSF $0.0361 \pm 0.0070$ |

where  $N$  is the total number of dark matter particles inside  $r_{\Delta_c}$ , the radius which encloses matter having average density  $\Delta_c$  times the critical density;  $v_{p,i}$  is the  $i$ -th velocity component ( $i = x, y, z$ ) of the  $p$ -th dark matter particle inside  $r_{\Delta_c}$ ; and  $\bar{v}_i$  is the peculiar velocity of the cluster is defined to be the mass-weighted average of all dark matter particles within  $r_{\Delta_c}$ . We have also calculated the cluster velocity using velocities of all species (dark matter, stars and gas), and it agrees with the average velocities of dark matter to within a few percent for most clusters, since baryons are only a minor fraction of the total cluster mass. We weigh the mean and variance by dark matter particle mass but it is insensitive to whether mass-weighted or number-weighted is used within  $r_{\Delta_c}$ . We take the cluster center to be the location of the subhalo which has the

highest binding energy.

A power law is then fitted to the dark matter virial scaling relation using standard least square minimization:

$$\log \sigma_{\text{DM}}(M, z) = \log \sigma_{\text{DM},0} + \alpha \log \left( \frac{h(z)M_{\Delta_c}}{2 \times 10^{14} M_{\odot}} \right) \quad (2)$$

where  $h(z) = H(z)/100 \text{ km s}^{-1} \text{ Mpc}^{-1}$  is the normalized Hubble parameter which takes into the account of the redshift dependence of  $M_{\Delta_c}$ . Figure 1 shows the fitted velocity dispersion-mass relations of the CSF and the NR runs at  $z = 0, 0.6$ , and  $1.0$ . Table 2 reports the best fit parameters of the velocity dispersion-mass relations measured at  $\Delta_c = 200$  and  $500$ . The errors are estimated by generating 5000 bootstrap samples from the sixteen clusters at each redshift.

At  $\Delta_c = 500$ , the NR scaling relation is consistent with the self-similar scaling relation with no evolution. At  $\Delta_c = 200$ , the best-fitted NR scaling relation at  $z = 0$  differs slightly ( $2.6\sigma$ ) from that of Evrard et al. (2008) with  $\alpha = 0.3361 \pm 0.0026$  and  $\sigma_{\text{DM}}(M_{200c} = 10^{15} h^{-1} M_{\odot}) = 1082.9 \pm 4.0 \text{ km/s}$ . Note that results are fully consistent with the Evrard et al. (2008) relation if we limit our analyses to systems with the mass range ( $M > 10^{14} h^{-1} M_{\odot}$ ) adopted in their analysis. Larger number of simulated clusters is needed to explore remaining minute deviation from the self-similar relation.

The CSF scaling relations differ significantly from the NR relation at all redshifts. The baryon dissipation increases the velocity dispersion of dark matter, making the slope shallower in the CSF run compared to that of the NR run. Interestingly, the log-normal scatter is only 3-5%, and it is remarkably insensitive to input gas physics and redshift.

The breaking of self-similarity by baryon dissipation in the CSF runs is illustrated more clearly in Figure 2, which shows the ratio of dark matter velocity dispersion in the CSF run relative to the NR run,  $\sigma_{200c}^{\text{CSF}}/\sigma_{200c}^{\text{NR}}$ <sup>5</sup> as a function of halo

<sup>5</sup> As the same cluster in CSF and NR runs may have slightly differ-

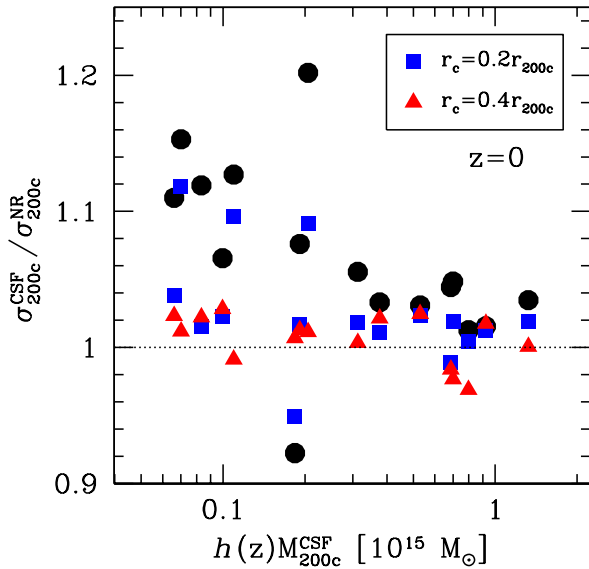


FIG. 2.— The ratios of velocity dispersions in the CSF and NR runs,  $\sigma_{200c}^{\text{CSF}}/\sigma_{200c}^{\text{NR}}$  as a function of cluster mass at  $z=0$ . Different symbols indicate velocity dispersions computed using DM particles in different annulus: [0-1] (circles), [0.2-1] (square) and [0.4-1] (triangles) in unit of  $r_{200c}$ .

mass at  $z=0$  on a cluster-by-cluster basis. For almost all halos, the inclusion of baryonic physics leads to an increase in dark matter velocity dispersion, and the effect is greater for lower mass systems. We find that this bias is of the order  $\sim 10\% - 15\%$  for  $M_{200c} \simeq 6 \times 10^{13} h^{-1} M_{\odot}$ , compared to 6% for  $M_{200c} > 3 \times 10^{14} h^{-1} M_{\odot}$ . This is because gas in lower mass halos is at a lower virial temperature and thus capable of cooling more efficiently to form stars. We find the same trend at higher redshift. Note that there is one outlier (CL5) which shows a decrease in the velocity dispersion in the CSF run. This is due to fast moving subhalos in the NR run that have already merged with the central subhalo in the CSF run. Another outlier in the opposite direction (CL6) has a  $\sim 20\%$  increase in velocity dispersion. This is also due to a similar merging event in the CSF, boosting its velocity dispersion.

We further show that the change in velocity dispersion is largely due to the baryon dissipation in the central regions of clusters. To illustrate this, we also compute velocity dispersions by excluding the central regions of clusters in Figure 2. This shows that differences in velocity dispersions in the CSF and NR runs become smaller when we apply central exclusion. Excluding  $r < 0.2r_{200c}$  reduces the differences in the CSF and NR to about 4% on most systems. The bias is even smaller (less than 2%) on all systems if we exclude the central  $r < 0.4r_{200c}$ . This illustrates that the increase in  $\sigma_{200c}$  is mainly driven by the increase in velocities in the inner regions of CSF groups and clusters.

Figure 3 shows the velocity dispersion profiles averaged over the 16 clusters at  $z=0$  and  $z=1$  for both CSF and NR runs. Note that the mass dependence seen in Figure 2 is explicitly taken out by dividing the circular velocity  $v_{200c}$ . The dark matter velocity dispersion of CSF clusters increases towards smaller radii compared to their NR counterparts. The change in the shape of the velocity dispersion profile is a di-

ent  $M_{200c}$ , we normalize each  $\sigma_{200c}$  with the circular velocity  $v_{200c} \equiv \sqrt{GM_{200c}/r_{200c}}$ .

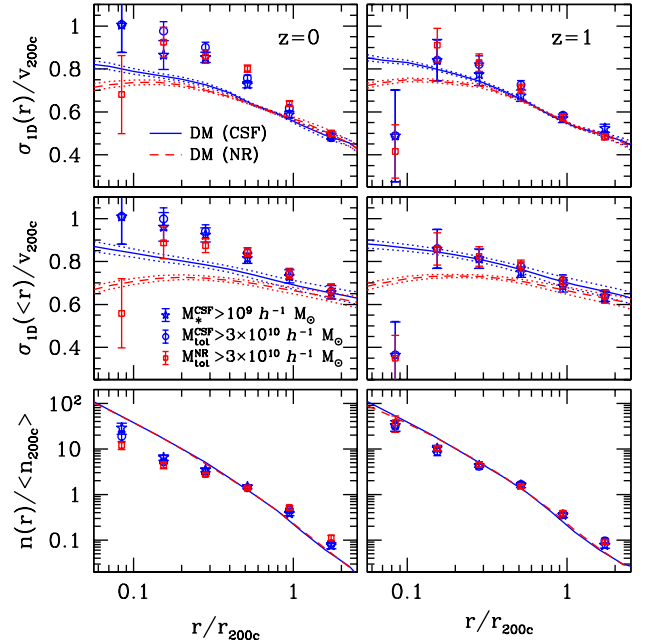


FIG. 3.— Average DM velocity dispersion profiles for the sixteen clusters at  $z=0$  (left-panels) and  $z=1$  (right-panels) for CSF (blue solid lines) and NR (red dashed lines) runs. Dotted lines are the corresponding  $1\sigma$  errors. The top panels show 1-D differential velocity dispersion profiles; the middle panels show the 1-D cumulative velocity dispersion profiles; the bottom panels show the corresponding number density profiles. Also plotted are profiles for CSF cluster galaxies (blue star), CSF subhalos (blue circle) and NR subhalos (red squares).

rect consequence of the enhancement of dark matter density caused by adiabatic contraction reported previously based on our simulations (Gnedin et al. 2004): as gas cools and condenses towards the center, it deepens the central potential and drags dark matter inward.

Note that we have assumed dark matter velocity dispersion to be isotropic. This, however, is not a completely valid assumption. In fact, some level of velocity anisotropy is expected for collisionless dark matter particles (Cole & Lacey 1996; Carlberg et al. 1997; Colín et al. 2000; Hansen & Moore 2006). Cluster galaxies are also collisionless as they have relaxation time greater than the Hubble time. Velocity anisotropy is therefore an important ingredient in the dynamical mass estimates. The anisotropy is commonly quantified by the anisotropy parameter  $\beta$ , defined as

$$\beta \equiv 1 - 0.5\sigma_t^2/\sigma_r^2, \quad (3)$$

where  $\sigma_r$  and  $\sigma_t$  are the radial and tangential velocity dispersions respectively. The definition of  $\sigma$  follows from Eq. (1), where contribution of mean velocities, which is non-zero beyond the virial radius, is included.

We therefore use our simulations to study the velocity anisotropy of dark matter as well as galaxies in groups and clusters. Figure 4 shows that dark matter velocity is nearly isotropic in the inner region of halo at  $0.1r_{200c}$ , and it becomes increasingly radial at larger radii (e.g.,  $\beta = 0.3$  at  $0.5r_{200c}$  and  $\beta = 0.35$  at  $r_{200c}$ ). Interestingly, we find that the dark matter velocity anisotropy profile is almost unaffected by the addition of cooling, star formation and feedback and insensitive to redshift between  $z=0$  and 1. The CSF velocity anisotropy is only slightly lower than that of the NR one. This makes sense given that the velocity anisotropy profile is only dependent on the slope of the density profile at large radii (Hansen & Moore 2006), where the effect of baryon dissipation is small.

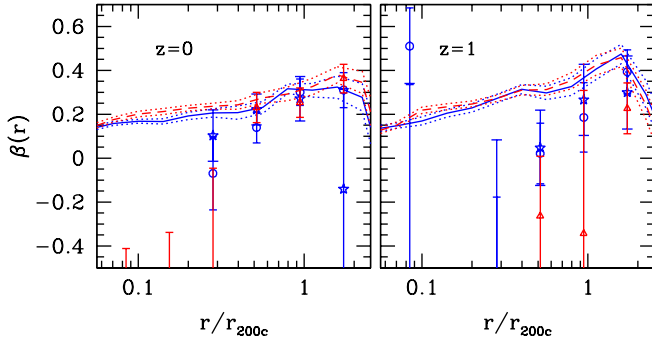


FIG. 4.— The average velocity anisotropy profiles. The notations are the same as Figure 3.

Finally, Evrard et al. (2008) show that low resolution can bias the slope of the scaling relation high. Their resolution studies indicate that the calibration of the virial scaling relation is not affected by resolution if clusters are resolved with more than  $10^5$  dark matter particles. In this work, we ensured that all groups and clusters used in our analyses are resolved with greater than  $3 \times 10^5$  particles. Thus, the resolution of our simulations is sufficient for the virial scaling relation work. The magnitude of the baryon dissipation, on the other hand, depends sensitively on the cooled gas fractions in simulations. Given that the current simulations suffer from the overcooling problem (e.g., Borgani & Kravtsov 2009), the effect of baryon dissipation in this work should be taken as an *upper limit*.

### 3.2. Velocity Bias

Since dark matter velocities are not directly observable, galaxies are used as tracers of the dynamics of underlying dark matter. Velocity dispersion of cluster galaxy  $\sigma_{\text{gal}}$ , however, is believed to be a “biased” tracer of the dark matter dynamics,  $\sigma_{\text{DM}}$  (Carlberg et al. 1990; Evrard et al. 1994; Frenk et al. 1996; Colín et al. 2000; Ghigna et al. 2000; Springel et al. 2001; Faltenbacher et al. 2005; Faltenbacher & Diemand 2006; Benatov et al. 2006). This velocity bias is often defined as,

$$b_v \equiv \frac{\sigma_{\text{gal}}}{\sigma_{\text{DM}}}, \quad (4)$$

where, as before, the one-dimensional velocity dispersions of both galaxies and dark matter are calculated assuming isotropy (i.e., Eq. (1)).

Figure 5 shows the velocity bias for both the CSF and NR runs. Following Nagai & Kravtsov (2005), we select subhalos using their total bound mass ( $M_{\text{tot}} \geq 3 \times 10^{10} h^{-1} M_{\odot}$ ) and stellar mass ( $M_* \geq 10^9 h^{-1} M_{\odot}$ ). In the NR runs, we only have the first sample, since there are no stars in these simulations. Results are summarized in the Table 3.

A main finding is that the velocity bias depends on how galaxies are selected. In the NR runs, we select subhalo using their current total bound mass and find that there is a positive bias of about 10% at all redshifts. This is in good agreement with the positive velocity bias of  $\approx 10\% - 15\%$  for dark matter subhalos in  $N$ -body simulations (Colín et al. 2000; Diemand et al. 2004; Gao et al. 2004). This positive velocity bias arises because selection of subhalos using their current bound mass radially biases the resulting sample to larger radii (Nagai & Kravtsov 2005). This selection also biases the sample by including more recently accreted subhalos which have larger velocity dispersions. Tidal disruption can lead to not only mass loss but also complete disruption

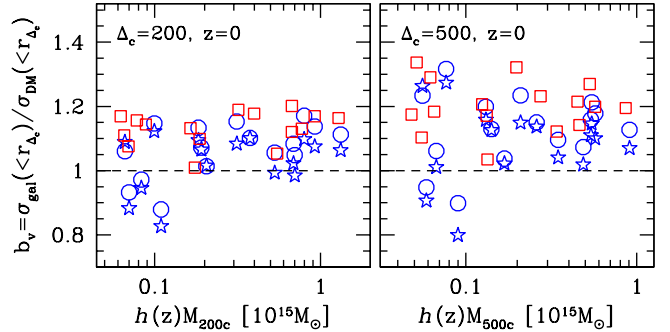


FIG. 5.— *Left panel* shows the velocity bias for  $\Delta_c = 200$  at  $z = 0$ , while the *right panel* shows the same for  $\Delta_c = 500$ . For each panel, the red squares represent the velocity bias for the NR subhalos selected using their current total bound mass of  $\geq 3 \times 10^{10} h^{-1} M_{\odot}$ , the blue circles are velocity bias for CSF subhalos selected with the same mass threshold. Blue stars show the velocity bias for the CSF subhalos selected using their stellar masses with threshold  $M_* \geq 10^9 h^{-1} M_{\odot}$ . We refer reader to the Table 3 for the mean velocity bias and  $1 - \sigma$  scatter at higher redshifts.

(or, equivalently, to mass loss that brings subhalo mass below resolution of simulation). The disrupted subhalos tend to be biased towards smaller radii and cannot be recovered by any selection criterion. It is generally thought that dissipation should enhance the survival of subhalos, although recent simulations show that effect is not as large as has been previously thought (Nagai & Kravtsov 2005; Macciò et al. 2006). Indeed, the numbers in Table 3 show that using the same subhalo selection criteria in the CSF runs the velocity bias is noticeably smaller (by a few percents). This means that baryon dissipation makes subhalos somewhat less susceptible to tidal disruption in the inner regions of groups and clusters.

In the CSF runs, we also select galaxies based on their stellar mass. Interestingly, galaxies selected this way shows almost *no* velocity bias. The selection criteria are important here because stars formed in the inner regions of galactic-size halos are tightly bound to the system and are more resistant to tidal mass loss (Nagai & Kravtsov 2005). This also explains why the bias is generally smaller at higher redshifts, where galaxies has not yet had the time to experience significant tidal mass loss (e.g., Conroy et al. 2006). This is also consistent with the previous results that find that both radial and velocity biases of subhalos largely disappear if subhalos are selected using their properties at the accretion epoch, unaffected by tidal stripping (Nagai & Kravtsov 2005; Faltenbacher & Diemand 2006). Moreover, this explains why the bias is slightly higher in the inner region (e.g.,  $\Delta_c = 500$ ), where the tidal effects should be more significant.

The importance of how subhalos are selected is further highlighted in Figure 3, which compares galaxy velocity dispersion profiles (*points with errorbars*) to the velocity dispersion profiles of dark matter particles, indicated by lines. The figure shows that velocity dispersions of galaxies are generally higher than those of dark matter in the radial range  $0.1 < r/r_{200c} < 1$ . The velocity bias is slightly larger when galaxies are selected using their current total mass, rather than their stellar mass. The figure also illustrates that both velocity and spatial biases are smaller at higher redshifts, where the tidal stripping and disruption had not yet had time to affect the masses of subhalos, and hence their spatial distribution and overall velocity dispersion.

For high-redshift objects, the number of cluster galaxies  $N_{\text{gal}}$  is often too limited for reliable dynamical mass. Using CSF simulations, we quantify how well one can estimate dark

TABLE 3  
VELOCITY BIAS

| mean $\pm 1\text{-}\sigma$ error | $\Delta_c = 200$  |                   |                   |
|----------------------------------|-------------------|-------------------|-------------------|
|                                  | $z = 0.0$         | $z = 0.6$         | $z = 1.0$         |
| $b_{v,sub}^{NR}$                 | $1.131 \pm 0.022$ | $1.063 \pm 0.036$ | $1.073 \pm 0.032$ |
| $b_{v,sub}^{CSF}$                | $1.067 \pm 0.021$ | $1.050 \pm 0.021$ | $1.032 \pm 0.024$ |
| $b_{v,sub}^{CSF}$                | $1.029 \pm 0.022$ | $0.993 \pm 0.032$ | $0.971 \pm 0.033$ |
| $b_{v,gal}^{CSF} (N_{gal} = 3)$  | $0.796 \pm 0.070$ | $0.792 \pm 0.055$ | $0.772 \pm 0.065$ |
| $b_{v,gal}^{CSF} (N_{gal} = 5)$  | $0.857 \pm 0.042$ | $0.783 \pm 0.053$ | $0.792 \pm 0.047$ |
| $b_{v,gal}^{CSF} (N_{gal} = 10)$ | $0.964 \pm 0.035$ | $0.894 \pm 0.027$ | $0.856 \pm 0.047$ |
| $b_{v,gal}^{CSF} (N_{gal} = 20)$ | $0.976 \pm 0.025$ | $0.969 \pm 0.027$ | $0.957 \pm 0.037$ |
|                                  | $\Delta_c = 500$  |                   |                   |
|                                  | $z = 0.0$         | $z = 0.6$         | $z = 1.0$         |
| $b_{v,sub}^{NR}$                 | $1.200 \pm 0.021$ | $1.084 \pm 0.043$ | $1.116 \pm 0.039$ |
| $b_{v,sub}^{CSF}$                | $1.128 \pm 0.028$ | $1.084 \pm 0.021$ | $1.078 \pm 0.025$ |
| $b_{v,sub}^{CSF}$                | $1.083 \pm 0.031$ | $1.018 \pm 0.034$ | $1.020 \pm 0.028$ |
| $b_{v,gal}^{CSF} (N_{gal} = 3)$  | $0.811 \pm 0.077$ | $0.756 \pm 0.066$ | $0.816 \pm 0.067$ |
| $b_{v,gal}^{CSF} (N_{gal} = 5)$  | $0.945 \pm 0.052$ | $0.821 \pm 0.052$ | $0.887 \pm 0.057$ |
| $b_{v,gal}^{CSF} (N_{gal} = 10)$ | $1.013 \pm 0.043$ | $0.928 \pm 0.037$ | $0.958 \pm 0.039$ |
| $b_{v,gal}^{CSF} (N_{gal} = 20)$ | $1.030 \pm 0.035$ | $1.022 \pm 0.019$ | $1.067 \pm 0.037$ |

matter velocity dispersion using a limited number of galaxies. Specifically, we compute the velocity bias using 3, 5, 10 and 20 most massive galaxies (excluding the central galaxy) in our CSF halos. The results are summarized in Table 3. Our analysis shows that galaxy velocity dispersion tends to exhibit less bias for larger number of galaxies. At  $z = 0$ , galaxy velocity dispersion is essentially unbiased (i.e.,  $b_v = 1$ ) within  $1\sigma$  for  $N_{gal} > 10$  at both  $\Delta_c = 200$  and 500. At higher redshifts, larger number of galaxies are required to achieve unbiased estimate. Our analyses indicate that the galaxy velocity dispersions are unbiased within  $2\sigma$  for  $N_{gal} \geq 20$  at  $z = 0.6$  and 1. A larger sample of simulated clusters are required to confirm the remaining bias at a level of 5% at these redshifts. Moreover, our results clearly show that the velocity bias is significant for  $N_{gal} < 10$  galaxies. This is because the more massive galaxies reside nearer to the inner region due to dynamical friction and hence have lower velocities.

#### 4. SUMMARY AND DISCUSSION

In this work we investigate the effect of baryon dissipation on the scaling relation between total mass and velocity dispersion, and the velocity bias of galaxies in clusters. To this end, we use a representative set of self-consistent cosmological cluster simulations that follow the formation and evolution of galaxies by taking into account effects of gas cooling, star formation, and feedback.

We confirm that the virial scaling relation of dark matter exhibits a remarkable degree of self-similarity with log-normal

scatter of only 5%. The virial scaling relation in our non-radiative hydrodynamical simulations is consistent with that of the dissipationless simulations presented by Evrard et al. (2008). This demonstrates that the virial scaling relation has now been calibrated at a level of *a few percent* in the non-radiative regime.

We show that the largest source of systematic uncertainty in the intrinsic virial scaling relation calibration lies in our understanding of baryonic physics. Using numerical simulation that include the physics of galaxy formation, we find that the baryon dissipation increases dark matter velocity dispersion of groups and clusters at the level of  $\sim 4\%$  to  $10\%$  due to adiabatic contraction of dark matter in the central regions. Our simulations indicate that this effect is more pronounced in lower mass systems where gas cooling and star formation are more efficient than massive systems. Note, however, that the effect of baryon dissipation in this work should be taken as an upper limit, because the current simulations suffer from the overcooling problem (e.g., Borgani & Kravtsov 2009). Despite this problem, we find that the scatter in the virial scaling relation is very tight (only  $\sim 5\%$ ), independent of mass and redshift, and insensitive to details to input cluster physics.

In practice, the dark matter virial scaling relation is not directly accessible to observations. Instead, observers rely on galaxies as tracers of the underlying distribution and dynamics of matter. Thus, the bias in the velocity dispersions of galaxies with respect to that of dark matter is one of the main sources of systematic uncertainty in the mass estimates of galaxy clusters. Previous works based on  $N$ -body simulations have shown that dark matter “subhalos” in simulations exhibits a positive velocity bias, because slow subhalos are much less common, due to physical disruption by gravitational tides early in the merging history (e.g., Colin et al. 2000; Diemand et al. 2004; Gao et al. 2004).

In this work, we show that the galaxy velocity bias, in fact, depends on how galaxies (“subhalos”) are selected in simulations. Using the self-consistent cluster simulations, we find that galaxies selected based on their stellar mass exhibit no velocity bias. Moreover, we find that the observational estimates of galaxy velocity dispersion with more than twenty most massive galaxies in groups and clusters is an unbiased tracer of the dynamics of underlying matter.

EL and AK are supported by the NSF grant AST-0708154, by NASA grant NAG5-13274, and by Kavli Institute for Cosmological Physics at the University of Chicago through grant NSF PHY-0551142 and an endowment from the Kavli Foundation. This work made extensive use of the NASA Astrophysics Data System and arXiv.org preprint server.

#### REFERENCES

- Arnaud, M. & Evrard, A. E. 1999, MNRAS, 305, 631  
 Becker, M. R., McKay, T. A., Koester, B., Wechsler, R. H., Rozo, E., Evrard, A., Johnston, D., Sheldon, E., Annis, J., Lau, E., Nichol, R., & Miller, C. 2007, ApJ, 669, 905  
 Benatov, L., Rines, K., Natarajan, P., Kravtsov, A., & Nagai, D. 2006, MNRAS, 370, 427  
 Biviano, A. 2000, in Constructing the Universe with Clusters of Galaxies  
 Biviano, A. & Girardi, M. 2003, ApJ, 585, 205  
 Biviano, A., Murante, G., Borgani, S., Diaferio, A., Dolag, K., & Girardi, M. 2006, A&A, 456, 23  
 Biviano, A. & Poggianti, B. M. 2009, A&A, 501, 419  
 Blumenthal, G. R., Faber, S. M., Flores, R., & Primack, J. R. 1986, ApJ, 301, 27  
 Borgani, S. & Kravtsov, A. 2009, ASL in press (arxiv/0906.4370)  
 Carlberg, R. G., Couchman, H. M. P., & Thomas, P. A. 1990, ApJ, 352, L29  
 Carlberg, R. G., Yee, H. K. C., & Ellingson, E. 1997, ApJ, 478, 462  
 Chen, J., Kravtsov, A. V., Prada, F., Sheldon, E. S., Klypin, A. A., Blanton, M. R., Brinkmann, J., & Thakar, A. R. 2006, ApJ, 647, 86  
 Coil, A. L., Gerke, B. F., Newman, J. A., Ma, C.-P., Yan, R., Cooper, M. C., Davis, M., Faber, S. M., Guhathakurta, P., & Koo, D. C. 2006, ApJ, 638, 668  
 Cole, S. & Lacey, C. 1996, MNRAS, 281, 716

- Colín, P., Klypin, A. A., & Kravtsov, A. V. 2000, *ApJ*, 539, 561
- Conroy, C., Wechsler, R. H., & Kravtsov, A. V. 2006, *ApJ*, 647, 201
- Diaferio, A. 1999, *MNRAS*, 309, 610
- Diaferio, A. & Geller, M. J. 1997, *ApJ*, 481, 633
- Diaferio, A., Geller, M. J., & Rines, K. J. 2005, *ApJ*, 628, L97
- Diemand, J., Moore, B., & Stadel, J. 2004, *MNRAS*, 352, 535
- Evrard, A. E., Bialek, J., Busha, M., White, M., Habib, S., Heitmann, K., Warren, M., Rasia, E., Tormen, G., Moscardini, L., Power, C., Jenkins, A. R., Gao, L., Frenk, C. S., Springel, V., White, S. D. M., & Diemand, J. 2008, *ApJ*, 672, 122
- Evrard, A. E., Summers, F. J., & Davis, M. 1994, *ApJ*, 422, 11
- Faltenbacher, A. & Diemand, J. 2006, *MNRAS*, 369, 1698
- Faltenbacher, A., Kravtsov, A. V., Nagai, D., & Gottlöber, S. 2005, *MNRAS*, 358, 139
- Frenk, C. S., Evrard, A. E., White, S. D. M., & Summers, F. J. 1996, *ApJ*, 472, 460
- Gao, L., De Lucia, G., White, S. D. M., & Jenkins, A. 2004, *MNRAS*, 352, L1
- Ghigna, S., Moore, B., Governato, F., Lake, G., Quinn, T., & Stadel, J. 2000, *ApJ*, 544, 616
- Girardi, M., Giuricin, G., Mardirossian, F., Mezzetti, M., & Boschin, W. 1998, *ApJ*, 505, 74
- Gnedin, O. Y., Kravtsov, A. V., Klypin, A. A., & Nagai, D. 2004, *ApJ*, 616, 16
- Hansen, S. H. & Moore, B. 2006, *New Astronomy*, 11, 333
- Heisler, J., Tremaine, S., & Bahcall, J. N. 1985, *ApJ*, 298, 8
- Hernquist, L., Katz, N., & Weinberg, D. H. 1995, *ApJ*, 442, 57
- Kaiser, N. 1986, *MNRAS*, 222, 323
- Katgert, P., Biviano, A., & Mazure, A. 2004, *ApJ*, 600, 657
- Klypin, A., Kravtsov, A. V., Bullock, J. S., & Primack, J. R. 2001, *ApJ*, 554, 903
- Kravtsov, A. V. 1999, PhD thesis, New Mexico State University
- Kravtsov, A. V., Klypin, A., & Hoffman, Y. 2002, *ApJ*, 571, 563
- Macciò, A. V., Moore, B., Stadel, J., & Diemand, J. 2006, *MNRAS*, 366, 1529
- Markevitch, M. 1998, *ApJ*, 504, 27
- McKay, T. A., Sheldon, E. S., Johnston, D., Grebel, E. K., Prada, F., Rix, H.-W., Bahcall, N. A., Brinkmann, J., Csabai, I., Fukugita, M., Lamb, D. Q., & York, D. G. 2002, *ApJ*, 571, L85
- Nagai, D. & Kravtsov, A. V. 2005, *ApJ*, 618, 557
- Nagai, D., Kravtsov, A. V., & Vikhlinin, A. 2007a, *ApJ*, 668, 1
- Nagai, D., Vikhlinin, A., & Kravtsov, A. V. 2007b, *ApJ*, 655, 98
- Osmond, J. P. F. & Ponman, T. J. 2004, *MNRAS*, 350, 1511
- Pratt, G. W., Croston, J. H., Arnaud, M., & Böhringer, H. 2009, *A&A*, 498, 361
- Rines, K. & Diaferio, A. 2006, *AJ*, 132, 1275
- Rines, K., Diaferio, A., & Natarajan, P. 2007, *ApJ*, 657, 183
- Rines, K., Geller, M. J., Kurtz, M. J., & Diaferio, A. 2003, *AJ*, 126, 2152
- Rudd, D. H., Zentner, A. R., & Kravtsov, A. V. 2008, *ApJ*, 672, 19
- Sellwood, J. A. & McGaugh, S. S. 2005, *ApJ*, 634, 70
- Slosar, A., Seljak, U., & Tasitsiomi, A. 2006, *MNRAS*, 366, 1455
- Smith, S. 1936, *ApJ*, 83, 23
- Springel, V., White, S. D. M., Tormen, G., & Kauffmann, G. 2001, *MNRAS*, 328, 726
- van der Marel, R. P., Magorrian, J., Carlberg, R. G., Yee, H. K. C., & Ellingson, E. 2000, *AJ*, 119, 2038
- Voit, G. M. 2005, *Reviews of Modern Physics*, 77, 207
- Zeldovich, Y. B., Klypin, A. A., Khlopov, M. Y., & Chechetkin, V. M. 1980, *Soviet J. Nucl. Phys.*, 31, 664
- Zwicky, F. 1933, *Helvetica Physica Acta*, 6, 110
- . 1937, *ApJ*, 86, 217